Collision Avoidance Method of Humanoid Robot With Arm Force

Eijiro Ohashi, Takahiro Aiko, Toshiaki Tsuji, *Student Member, IEEE*, Hiroaki Nishi, *Member, IEEE*, and Kouhei Ohnishi, *Fellow, IEEE*

***Abstract*—This paper describes a collision avoidance method for a biped robot with an upper body. We propose a method wherein the robot stops in front of an obstacle by generating arm force. When the robot detects the obstacle by the arm tip, it should stop short of the obstacle to avoid crash. Hence, we propose trajectory planning in consideration of the pushing force of the arm. The arm force is controlled to be generated as a function of the distance from the robot body to the obstacle. The closer the robot approaches the obstacle, the larger the arm force becomes. As a result, the robot can stop by utilizing the arm force. In case the obstacle is unmovable, the robot can stop by exerting arm force. If it is movable, the robot can continue walking by pushing it. In this paper, the linear inverted pendulum mode (LIPM) and the idea of orbital energy are introduced, and then, we extend LIPM and orbital energy in consideration of the dynamics of the arm force. The extended orbital energy is utilized to discriminate whether the robot can stop or not and to modify the trajectory of the robot to avoid collision.**

***Index Terms*—Arm force, biped robot, collision avoidance, humanoid robot, pushing motion, trajectory planning, walking robot.**

I. Introduction

LEGGED ROBOTS have been developed in recent years. One of the very important features of legged robots is that they can step on arbitrary landing points. Therefore, legged robots have the ability to step over obstacles, such as holes, steps, and bumps. From this point of view, they are superior to robots with wheels or crawlers in traveling around a human environment that has rugged terrain.

Biped robots have already been able to walk just like human beings. Löffler *et al.* investigated a sensor system and the control schemes of their humanoid robot [1]. Tan *et al.* studied a method for a humanoid robot to learn multiple tasks in an unknown environment [2]. Furthermore, biped robots have already been able to run [3]–[6]. Much research about biped robots has focused on walking motion itself. However, biped robots are expected not only to walk (or to run), but also to do some work using arms of upper bodies instead of those of human beings. Although walking motion has been investigated for about 30 years, cooperative motion between the upper body and the lower body has been discussed only for the last decade. In order that humanoid robots become valuable in human society, research about the cooperative motion should be further developed.

Harada *et al.* studied the zero moment point (ZMP) analysis of a humanoid robot under pushing motion [7]–[9]. The ZMP is an index that evaluates walking stability. They proposed the generalized ZMP, which takes into account the dynamics of the pushing force. They defined the fundamental ZMP trajectory based on a trajectory with no contact force on the arms. When the robot pushes an object, the fundamental ZMP trajectory is modified by a certain amount to walk stably. Hwang *et al.* studied the static stability of the motion of pushing a wall and the motion of twisting a valve while the humanoid robot does not change the foot position [10]. Yoshida *et al.* investigated a humanoid robot that has tasks on the arms [11], [12]. When external force is small or the arm tip moves in narrow space, the robot remains in the double support phase. On the other hand, when large force affects the robot or the arm tip has to move in wide range, the robot makes a step to recover its stability.

As mentioned above, most researchers focused on how humanoid robots keep on walking (or standing) stably when the arms of the upper body do some particular work. An important aim of these researches is to make the arms do desired work. As a result, the upper body and the lower body have separate tasks, e.g., pushing and walking.

Kuniyoshi *et al.* studied dynamic roll-and-rise motion, taking into account the dynamics of the upper body of a humanoid robot [13], [14]. The action of the upper body is considered as an important element to accomplish the dynamic roll-and-rise motion. The upper and lower bodies have the same motive, i.e., to achieve the desired motion.

In this paper, we also consider the pushing motion of the arms of a humanoid robot. However, arm force is exerted to support and to stabilize walking motion. The upper body has the same motive as the lower body. After contacting an obstacle, the robot stabilizes walking motion by utilizing arm force, and then, the robot does some work with the arms, e.g., pushing the obstacle. One of the aims of this paper is to utilize the arms to

Manuscript received November 12, 2005; revised February 28, 2006. This work was supported by the Institute of Electrical and Electronics Engineers.

E. Ohashi was with the Department of System Design Engineering, Faculty of Science and Technology, Keio University, Yokohama 223-8522, Japan. He is now with Canon Inc., Tokyo 146-8501, Japan (e-mail: ei2ro@sum.sd.keio.ac.jp).

T. Aiko was with the Department of System Design Engineering, Faculty of Science and Technology, Keio University, Yokohama 223-8522, Japan. He is now with the Plant Control Department, East Japan Works, JFE Steel Corporation, Kawasaki 210-0868, Japan (e-mail: aiko@sum.sd.keio.ac.jp).

T. Tsuji, H. Nishi, and K. Ohnishi are with the Department of System Design Engineering, Faculty of Science and Technology, Keio University, Yokohama 223-8522, Japan (e-mail: tsuji@sum.sd.keio.ac.jp; west@sd.keio.ac.jp; ohnishi@sd.keio.ac.jp).

Color versions of one or more of the figures in this paper are available online at http://ieeexplore.ieee.org.

Digital Object Identifier 10.1109/TIE.2007.894728

accomplish the desired walking motion. In addition, the arms are also used to detect the obstacle and to discriminate whether the obstacle is movable or not.

There is very little research that utilizes the arm force for stopping motion. Robots in unknown environments contact many objects, such as walls, doors, and human beings. We define these objects as "obstacles." If the arm tip detects the obstacle, the first thing the robot will do is to stop in front of it. However, modifying the walking trajectory needs enormous ankle torque if all energy of walking is suppressed only by the ankle torque. Unless the robot can generate enough ankle torque, it may crash to the obstacle. Even if the ankle torque can be generated sufficiently, walking motion may be destabilized. In either case, the robot cannot remain in a stable condition.

Therefore, we propose a trajectory planning of a humanoid robot with arm force. The robot pushes an obstacle using its arms in order not to crash against the obstacle. Under this motion, the arm force should be modified based on the distance from the obstacle. At the moment of contact, stiffness of the arm should be zero so that the robot has compliance with the obstacle. Thereafter, the arm force increases gradually to decelerate the robot body and to detect whether the obstacle is movable or not. Hence, the arm force is modified corresponding to the distance from the obstacle. It is appropriate for contact motion that the closer the robot approaches the obstacle, the larger the arm force should become. If the robot exerts sudden large arm force to the obstacle, it may move far away from the robot or it may be damaged. In this paper, the arm force is controlled to be in proportion with the distance from the obstacle.

In order to plan the trajectory, we develop the index of orbital energy [15] proposed by Kajita *et al.* In this paper, linear inverted pendulum mode (LIPM) is applied to generate a walking trajectory, and then, we extend the index of orbital energy by adding a term of arm force. Based on the extended index, the robot can modify the trajectory to avoid collision. In addition, we are able to predict whether a robot in a certain condition can stop short of the obstacle. When it is expected that the robot cannot stop, larger force should be exerted from the beginning of the contact. Consequently, the robot adapts to an unknown environment by modifying a walking trajectory appropriately.

We assume that contact motion between the obstacle and the arm tip is stable. The robot has no external sensors (visual sensor, ultrasonic sensor, and so on) to detect an obstacle beforehand. The robot can detect the obstacle only after the arm contacts it. The upper body and the lower body are coupled mechanically. We consider the motion of the robot in the sagittal plane.

This paper is organized as follows. In Section II, the model of the humanoid robot that has an upper body with arms is shown. In Section III, LIPM and its orbital energy are introduced. In Section IV, extending LIPM and the idea of orbital energy, we propose a collision avoidance method with pushing motion of the arms. Simulation results and experimental results are shown in Sections V and VI, respectively. Finally, this paper is concluded in Section VII.

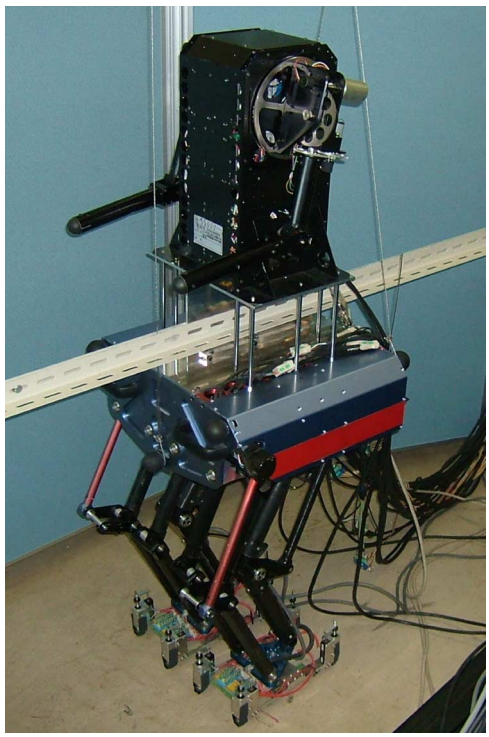

Fig. 1. Humanoid robot.

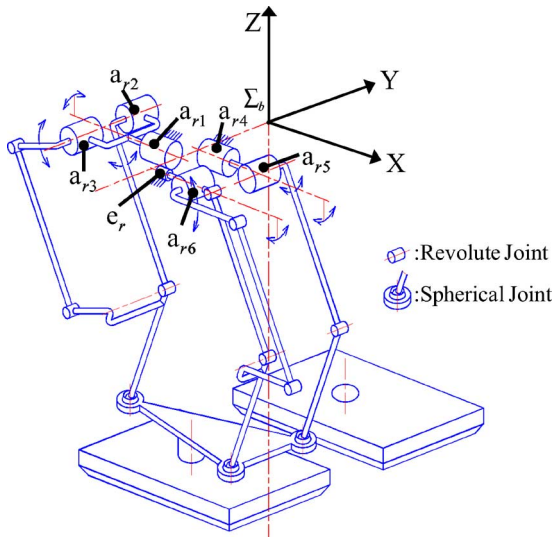

Fig. 2. Leg structure.

II. Modeling

Fig. 1 shows the humanoid robot. The legs of the robot have a parallel link mechanism. A feature of the parallel link mechanism is that all actuators of the legs exist at the trunk of the robot. It is reasonable to apply LIPM since the mass of the robot is concentrated at the trunk.

The structure of the leg is shown in Fig. 2. Each a is an active joint, and e is an encoder. Subscript r and i in a_{ri} and e_r represent right leg and joint i, respectively. The base coordinate system Σ_b is defined at the center of the located joint plane. Hereinafter, we represent only kinematics of the right leg and the right arm. Those of the left leg and the left arm can also be expressed in the same way.

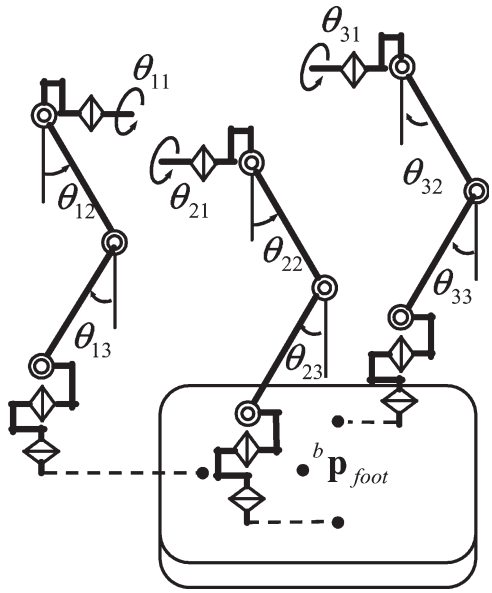

Fig. 3. Left leg model.

Inverse kinematics can be obtained as follows:

$$\boldsymbol{\theta}_{\mathrm{leg}} = \boldsymbol{F}\left({}^{b}\boldsymbol{p}_{\mathrm{foot}}, {}^{b}\boldsymbol{A}_{\mathrm{foot}}\right) \tag{1}$$

where Σ_b is the base coordinate system and $\boldsymbol{\theta}_{\mathrm{leg}}$ is the active joint angle vector $(= [\theta_{11}, \theta_{12}, \theta_{13}, \theta_{21}, \theta_{21}, \theta_{33}]^T)$ in Σ_b, as shown in Fig. 3. $\boldsymbol{F}(\cdot)$ is the function of kinematic relationship from the foot position and attitude to joint angles. ${}^{b}\boldsymbol{p}_{\mathrm{foot}} \in \Re^3$ is the position vector of each foot in Σ_b, and ${}^{b}\boldsymbol{A}_{\mathrm{foot}} \in \Re^{3\times 3}$ is the direction matrix, which expresses the posture of the foot in Σ_b.

The Jacobian matrix for the parallel link mechanism $\boldsymbol{J}_{\mathrm{leg}}$ is defined as follows:

$$\dot{\boldsymbol{\theta}}_{\mathrm{leg}} = \boldsymbol{J}_{\mathrm{leg}} \begin{bmatrix} {}^{b}\boldsymbol{p}_{\mathrm{foot}} \\ {}^{b}\boldsymbol{\omega}_{\mathrm{foot}} \end{bmatrix} \tag{2}$$

where $\boldsymbol{J}_{\mathrm{leg}}$ is the Jacobian matrix of the leg and ${}^{b}\boldsymbol{\omega}_{\mathrm{foot}} \in \Re^3$ is the angular velocity vector of the foot. The Jacobian matrix for the parallel link mechanism is unlike that of a serial link mechanism. Kinematics and dynamics of the leg are elaborated in [16].

The model of the upper body in the sagittal plane is shown in Fig. 4. In this paper, we simplify the structure of the robot by assuming that the robot has only one arm. In order to apply a robot with two arms, the only differentia is that arm force becomes half.

The arm tip position in Σ_b is represented as follows:

$${}^{b}\boldsymbol{x}_{\mathrm{tip}} = \begin{bmatrix} l_1 \cos\theta_1 + l_2 \cos(\theta_1 + \theta_2) + {}^{b}x_{\mathrm{sh}} \\ -l_1 \sin\theta_1 - l_2 \sin(\theta_1 + \theta_2) + {}^{b}z_{\mathrm{sh}} \end{bmatrix} \tag{3}$$

where

- ${}^{b}\boldsymbol{x}_{\mathrm{tip}}$ arm tip position vector $(= [{}^{b}x_{\mathrm{tip}}, {}^{b}z_{\mathrm{tip}}]^T)$ in Σ_b;
- ${}^{b}\boldsymbol{x}_{\mathrm{sh}}$ shoulder joint position vector $(= [{}^{b}x_{\mathrm{sh}}, {}^{b}z_{\mathrm{sh}}]^T)$ in Σ_b;
- $\boldsymbol{\theta}_{\mathrm{arm}}$ arm joint angle vector $(= [\theta_1, \theta_2]^T)$;
- l_i length of arm link i.

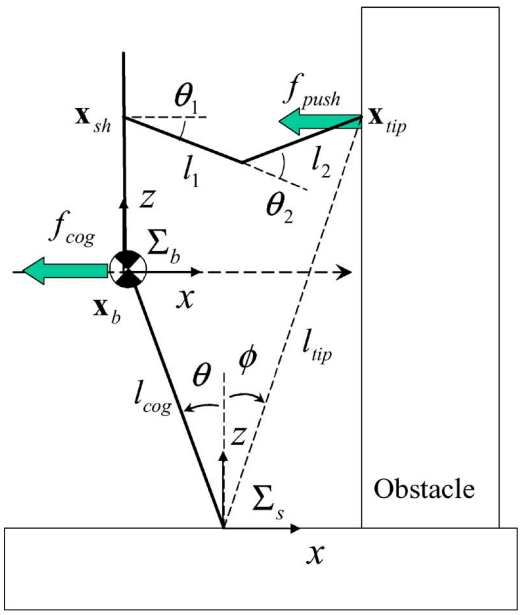

Fig. 4. Kinematic relationship.

Differentiating (3), we can obtain a Jacobian matrix of the arm $\boldsymbol{J}_{\mathrm{arm}}(\boldsymbol{\theta}_{\mathrm{arm}})$, i.e.,

$$\begin{aligned} &{}^{b}\dot{\boldsymbol{x}}_{\mathrm{tip}} \\ &\quad = \boldsymbol{J}_{\mathrm{arm}}(\boldsymbol{\theta}_{\mathrm{arm}})\dot{\boldsymbol{\theta}}_{\mathrm{arm}} \\ &\boldsymbol{J}_{\mathrm{arm}}(\boldsymbol{\theta}_{\mathrm{arm}}) \\ &\quad = \begin{bmatrix} -l_1 \sin\theta_1 - l_2 \sin(\theta_1 + \theta_2) & -l_2 \sin(\theta_1 + \theta_2) \\ -l_1 \cos\theta_1 - l_2 \cos(\theta_1 + \theta_2) & -l_2 \cos(\theta_1 + \theta_2) \end{bmatrix}. \end{aligned} \tag{4}$$

The relationship between joint torque and manipulating force at the tip of the arm is represented as follows:

$$\boldsymbol{\tau}_{\mathrm{push}} = \boldsymbol{J}_{\mathrm{arm}}(\boldsymbol{\theta}_{\mathrm{arm}})^T \boldsymbol{f}_{\mathrm{push}} \tag{5}$$

$$\begin{bmatrix} \tau_1 \\ \tau_2 \end{bmatrix} = \begin{bmatrix} -l_1 \sin\theta_1 - l_2 \sin(\theta_1 + \theta_2) \\ -l_2 \sin(\theta_1 + \theta_2) \end{bmatrix} f_{\mathrm{push},x} \tag{6}$$

$$= \begin{bmatrix} {}^{b}z_{\mathrm{tip}} - {}^{b}z_{\mathrm{sh}} \\ -l_2 \sin(\theta_1 + \theta_2) \end{bmatrix} f_{\mathrm{push},x} \tag{7}$$

where $\boldsymbol{\tau}_{\mathrm{push}} = [\tau_1, \tau_2]^T$ is a joint torque vector of the arm, and $\boldsymbol{f}_{\mathrm{push}} = [f_{\mathrm{push},x}, 0]^T$ is arm force vector exerted at the arm tip to the obstacle. In this paper, the robot is controlled to generate the arm force only in the horizontal direction, i.e., the robot pushes the obstacle horizontally. This is appropriate when LIPM is introduced since the center of gravity (COG) of the robot can be controlled to move horizontally.

Since the robot's legs have a smaller mass than that of the arms, as shown in Table I, the dynamics of the swing leg and the arms can be negligible, and the COG position of the robot scarcely varies. It is more appropriate to apply LIPM to parallel link robots than to serial link robots, since the robots with parallel link mechanism are more suitable to be approximated to an inverted pendulum.

TABLE I
PARAMETERS OF THE ROBOT

		Size[mm]	Mass[kg]
Upper Body	Body	173 × 200 × 560	6.0
	Upper Arm	200	0.7 × 2
	Lower Arm	230	0.3 × 2
Lower Body	Body	519 × 472 × 132	19.4
	Thigh	300	1.5 × 2
	Shin	300	0.5 × 2
	Foot	142 × 270 × 55	2.1 × 2

The relationship between (7) and the torque limit of each arm joint determines the maximum arm force in the horizontal direction $f_{\max}$, i.e.,

$$f_{\max} = \min\left[\left|\frac{\tau_{1,\max}}{{}^b z_{\rm tip} - {}^b z_{\rm sh}}\right|, \left|\frac{\tau_{2,\max}}{-l_2 \sin(\theta_1+\theta_2)}\right|\right] \tag{8}$$

where $f_{\max}$ is the maximum arm force in horizontal direction and $\boldsymbol{\tau}_{\max}$ is the arm joint torque limit vector $(= [\tau_{1,\max}, \tau_{2,\max}]^T)$. Hereinafter, we express each position in the supporting point coordinate system Σ_s, as shown in Fig. 4. The origin of Σ_s is defined at the ankle joint of the supporting leg. We define the point as the "supporting point." Variables in the Σ_s have no superscript on their left side. Each variable in Fig. 4 is represented as follows:

- Σ_s supporting point coordinate system;
- $\boldsymbol{x}_b$ COG position vector $(= [x_b, z_b]^T)$ in Σ_s;
- $\boldsymbol{x}_{\rm tip}$ arm tip position vector $(= [x_{\rm tip}, z_{\rm tip}]^T)$ in Σ_s;
- $l_{\rm cog}$ length from supporting point to COG;
- $l_{\rm tip}$ length from supporting point to arm tip;
- θ angle from vertical to COG around Σ_s;
- ϕ angle from vertical to arm tip around Σ_s;

where

$$l_{\rm tip} = \sqrt{x_{\rm tip}^2 + z_{\rm tip}^2} \tag{9}$$

$$z_b = l_{\rm cog} \cos\theta \tag{10}$$

$$z_{\rm tip} = l_{\rm tip} \cos\phi. \tag{11}$$

III. LIPM AND ORBITAL ENERGY

In this section, LIPM and the idea of orbital energy [15] proposed by Kajita *et al.* are introduced. In LIPM, a robot is modeled as an inverted pendulum, which has point mass (i.e., the COG of the robot). It is assumed that mass of the leg is negligible, and that the leg length can be variable. Consequently, the dynamics of the pendulum becomes very simple. We can control legged robots easily based on the simple model of LIPM.

When the COG height of the robot z_b is controlled to be constant, the acceleration of the mass of the pendulum is represented as follows:

$$\ddot{x}_b(t) = \frac{g}{z_b} \cdot x_b(t) \tag{12}$$

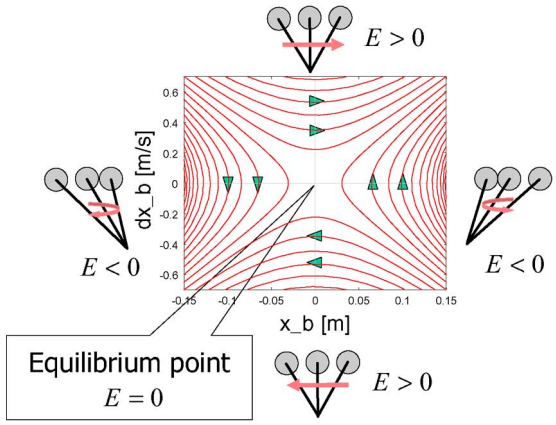

Fig. 5. Phase plane of LIPM.

where g is the gravity acceleration and t is time. The robot ideally needs no ankle torque as long as the robot tracks the trajectory of LIPM if the whole system of the robot can be assumed as a point mass system. An analytical solution of (12) can be derived as follows:

$$x_b(t) = x_{b0}\cosh(\omega t) + \frac{\dot{x}_{b0}}{\omega}\sinh(\omega t) \tag{13}$$

$$\dot{x}_b(t) = \left\{x_{b0}\sinh(\omega t) + \frac{\dot{x}_{b0}}{\omega}\cosh(\omega t)\right\}\omega \tag{14}$$

$$\omega = \sqrt{\frac{g}{z_b}}$$

where $x_{b0} = x_b(0)$ and $\dot{x}_{b0} = \dot{x}_b(0)$ are the boundary conditions.

Furthermore, orbital energy on LIPM is denoted as follows:

$$E = \frac{\dot{x}_b(t)^2}{2} - \frac{\omega^2 x_b(t)^2}{2} = \text{const.} \tag{15}$$

where E is the orbital energy. We can understand that orbital energy is the virtual energy of walking. The first term on the right-hand side represents kinetic energy of the COG. The second term on the right-hand side represents potential energy based on a virtual gravitational field.

When $E > 0$, the body swings from the minus side to the plus side in x-axis. $E = 0$ represents the equilibrium state. When $E < 0$, the body never goes over the supporting point. From this point of view, orbital energy is an index that discriminates whether the robot stops or not.

In addition, orbital energy can be obtained by the boundary conditions $[x_{b0} = x_b(0)$ and $\dot{x}_{b0} = \dot{x}_b(0)]$, as shown by the following equation:

$$E = \frac{\dot{x}_{b0}^2}{2} - \frac{\omega^2 x_{b0}^2}{2}. \tag{16}$$

Therefore, we can discriminate at the beginning of each step. The phase plane of $x_b(x)$ is shown in Fig. 5. The origin of the phase plane is the equilibrium point.

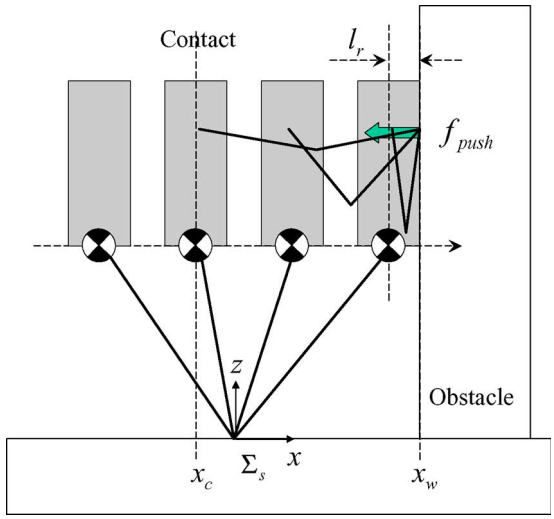

Fig. 6. Pushing motion of LIPM.

IV. Proposed Method

In this section, we propose a collision avoidance method with arm force. This method shows that the robot can stop in front of the obstacle by exerting the arm force. We will extend LIPM by adding the arm force and will extend the orbital energy [15] in consideration of arm force to discriminate whether the robot can stop short of the obstacle. Based on the extended orbital energy, we propose modifying the pushing force and the trajectory of the robot.

A. Extended LIPM

When the arm tip pushes the obstacle as shown in Fig. 6, $f_{\rm push}$ acts on the arm tip. For simplicity, we assume that the pushing force is generated only in the horizontal direction, i.e., $f_{{\rm push},x}$. This is appropriate when LIPM is introduced to keep the COG height constant.

We will consider the trajectory of the robot based on the COG motion. Therefore, $f_{\rm push}(=f_{{\rm push},x})$ should be transformed to $f_{\rm cog}$, which is the apparent force on the COG of the robot, as shown in Fig. 4. Since LIPM is introduced, the following equilibrium of moment around the supporting point is derived:

$$f_{\rm cog}\cos\theta\cdot l_{\rm cog}=f_{\rm push}\cos\phi\cdot l_{\rm tip}. \tag{17}$$

Substituting (10) and (11) in (17) yields

$$\therefore\quad f_{\rm cog}=\frac{z_{\rm tip}}{z_b}\cdot f_{\rm push} \tag{18}$$

where $f_{\rm cog}$ is the apparent force on COG. Considering the pushing force, we extend LIPM as follows:

$$\ddot{x}_b(t)=\frac{g}{z_b}\cdot x_b(t)-\frac{f_{\rm cog}}{m} \tag{19}$$

where m is the total mass of the robot. Note that the COG height remains constant and that no ankle torque is needed when the robot tracks the trajectory of (19). The ZMP of the robot is always on the supporting point if no ankle torque is generated. As a result, the walking motion is stable.

In unknown environments, a robot should not push an obstacle at the moment of contact, but should be compliant to the obstacle. Then, the robot increases the arm force gradually to stop and to discriminate whether the obstacle is movable or not. If the obstacle is unmovable like a wall, the robot must stop before the obstacle by utilizing the arm force. On the other hand, if the obstacle is movable like a door or other objects, the robot can push it and can walk forward.

From this point of view, in this paper, $f_{\rm push}$ is modified from zero to a certain value linearly in proportion to the distance from the obstacle. Hence, we introduce the following function of the pushing force:

$$\begin{aligned} f_{\rm push}&=k_{\rm arm}\left(x_b(t)-x_c\right)\\ k_{\rm arm}&=\frac{f_{\max}}{x_w-x_c-l_r}\end{aligned} \tag{20}$$

where

- x_w position of obstacle's surface;
- x_c COG position at the moment of contact, as shown in Fig. 6;
- l_r distance from COG to robot's front surface;
- $k_{\rm arm}$ spring coefficient of arm force;
- $f_{\max}$ maximum arm force.

l_r is determined by the mechanical structure of the robot. $f_{\max}$ is determined by (8).

From (18) and (20), $f_{\rm cog}$ can be expressed as

$$\begin{aligned} f_{\rm cog}&=k_{\rm cog}\left(x_b(t)-x_c\right)\\ k_{\rm cog}&=\frac{z_{\rm tip}}{z_b}\cdot k_{\rm arm}.\end{aligned} \tag{21}$$

Substituting (21) into (19) yields the generalized solution of (19), i.e.,

$$x_b(t)=\left(x_c+\frac{a_f}{\omega_f^2}\right)\cosh(\omega_f t)+\frac{\dot{x}_c}{\omega_f}\sinh(\omega_f t)-\frac{a_f}{\omega_f^2} \tag{22}$$

$$\dot{x}_b(t)=\left\{\left(x_c+\frac{a_f}{\omega_f^2}\right)\sinh(\omega_f t)+\frac{\dot{x}_c}{\omega_f}\cosh(\omega_f t)\right\}\omega_f \tag{23}$$

$$\omega_f=\sqrt{\frac{g}{z_b}-\frac{k_{\rm cog}}{m}}$$

$$a_f=\frac{k_{\rm cog}x_c}{m}.$$

When the robot contacts the obstacle, the trajectory of the conventional LIPM [(13) and (14)] should be switched to the trajectory with arm force [(22) and (23)]. On this trajectory planning, the COG locomotion is continuous in the velocity dimension.

After the contact occurs, the robot should stop in front of the obstacle. In order to discriminate whether it can stop before colliding to the obstacle, we introduce the index of orbital energy in Section IV-B.

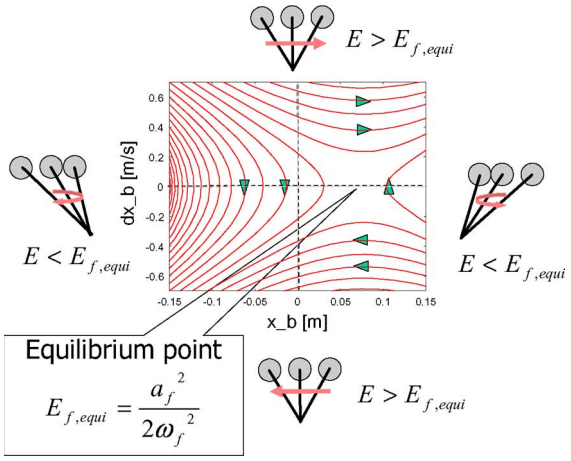

Fig. 7. Phase plane of LIPM with arm force ($k = 150$).

B. Extended Orbital Energy

We extend orbital energy in consideration of arm force. The extended orbital energy depending on (19) is derived as follows:

$$E_f = \frac{\dot{x}_b(t)^2}{2} - \frac{\omega_f^2 x_b(t)^2}{2} - a_f x_b(t) = \text{const.} \tag{24}$$

Then, we will derive an equilibrium point of (24). Setting $\dot{x}_b(t) = 0$ in (24) yields

$$E_f = -\frac{\omega_f^2}{2}\left(x_b(t) + \frac{a_f}{\omega_f^2}\right)^2 + \frac{a_f^2}{2\omega_f^2} \text{ when } \dot{x}_b(t) = 0. \tag{25}$$

The robot is in the equilibrium state when the orbital energy in (25) is the maximum, i.e., $x_b(t) = -a_f/\omega_f^2$. On this condition, the extended orbital energy on the equilibrium point is derived as

$$E_{f,\text{equi}} = \frac{a_f^2}{2\omega_f^2} \tag{26}$$

where $E_{f,\text{equi}}$ is the E_f on equilibrium point. When $E_f > E_{f,\text{equi}}$, the body swings from the minus side to the plus side in x-axis, i.e., the robot crashes to the obstacle. When $E_f < E_{f,\text{equi}}$, the body stops in front of the obstacle. When the robot is in the state that satisfies $E_f < E_{f,\text{equi}}$, the robot can stop in front of the obstacle by exerting the arm force. Aspects of the phase plane are shown in Fig. 7. $E_f = E_{f,\text{equi}}$ represents the equilibrium state. Note that the equilibrium point is shifted to the right, compared with Fig. 5. For example, if the robot has the same boundary conditions $\dot{x}_{b0} = 0.6$ and $x_{b0} = -0.1$, the robot in Fig. 5 (without arm force) goes over the supporting point. On the other hand, the robot in Fig. 7 (with arm force) goes backward. Considering the index of E_f, we can discriminate whether the robot stops in front of the obstacle.

C. Modification of Step Length

In this section, we derive the desired next step position of the swing leg.

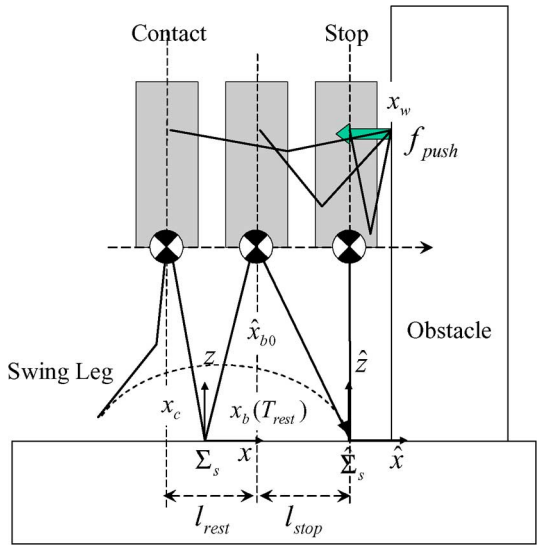

Fig. 8. Motion of next step.

In Section IV-D, we described that the extended orbital energy can be modified by exerting the arm force. By modifying the extended orbital energy, we can control the robot to avoid collision with the obstacle. Therefore, it is also important where the robot steps next, since orbital energy can be changed easily by modifying the next step length. In order to stop in front of the obstacle, the robot should make the next step at proper position.

The moment of contact is defined as t_c. After the contact occurs, the trajectory of the robot is switched from the conventional LIPM [(13) and (14)] to LIPM with arm force [(22) and (23)]. Then, we will modify a trajectory of the swing leg to accomplish a desired landing point. When the robot keeps a constant walking cycle T, boundary conditions (the COG position and velocity) of the next step are uniquely determined as $x_b(T_{\text{rest}})$ and $\dot{x}_b(T_{\text{rest}})$ in (22) and (23), respectively. Here, $T_{\text{rest}} = T - t_c$. We define each parameter in Fig. 8 as follows:

- t_c time at contact;
- T_{rest} duration from contact to the next step;
- l_{rest} distance from COG position at $t = t_c$ to at $t = T$;
- l_{stop} distance from COG position at $t = T$ to next supporting point of foot;
- $\hat{\Sigma}_s$ supporting point coordinate system of next step.

Here, l_{stop} determines the position of the next step. $l_{\text{rest}} = x_b(T) - x_b(t_c)$. We will evolve the following discussion on the assumption that $l_{\text{rest}} > 0$. In case that $l_{\text{rest}} \leq 0$, arm force is too large, and the robot should stop when the COG velocity becomes zero. If pushing force is too large, the strategy in Section IV-D should be applied.

Hereinafter, we consider the coordinate system of the next step $\hat{\Sigma}_s$, as shown in Fig. 8. Here, "^" denotes the coordinate system of the next step. For instance, the COG position during the next step is represented as $\hat{x}_b(t)$. The boundary conditions are determined as follows:

$$\hat{x}_{b0} = -l_{\text{stop}}$$
$$\dot{\hat{x}}_{b0} = \dot{x}_b(T_{\text{rest}}).$$

Apparent force on the COG is obtained as

$$\hat{f} = k_{\mathrm{cog}} \left(\hat{x}_b(t) + l_{\mathrm{stop}} + l_{\mathrm{rest}} \right) \tag{27}$$

where $-l_{\mathrm{stop}} \leq \hat{x}_b(t)$. The generalized solution can be derived on these boundary conditions, i.e.,

$$\hat{x}_b(t) = \left(\hat{x}_{b0} + \frac{\hat{a}_f}{\omega_f^2} \right) \cosh(\omega_f t) + \frac{\dot{\hat{x}}_{b0}}{\omega_f} \sinh(\omega_f t) - \frac{\hat{a}_f}{\omega_f^2} \tag{28}$$

$$\dot{\hat{x}}_b(t) = \left\{ \left(\hat{x}_{b0} + \frac{\hat{a}_f}{\omega_f^2} \right) \sinh(\omega_f t) + \frac{\dot{\hat{x}}_{b0}}{\omega_f} \cosh(\omega_f t) \right\} \omega_f \tag{29}$$

$$\hat{a}_f = - \frac{k_{\mathrm{cog}}(l_{\mathrm{stop}} + l_{\mathrm{rest}})}{m}.$$

Extended orbital energy on the next step $\hat{E}_f$ can be derived as

$$\hat{E}_f = \frac{\dot{\hat{x}}_b(t)^2}{2} - \frac{\omega_f^2 \hat{x}_b(t)^2}{2} - \hat{a}_f \hat{x}_b(t). \tag{30}$$

Setting $\dot{\hat{x}}_b(t) = \dot{\hat{x}}_{b0}$ and $\hat{x}_b(t) = -l_{\mathrm{stop}}$ in (30) derives $\hat{E}_f$.

The COG of the robot stops just above the supporting point when $\hat{E}_f$ is equal to 0. In this case, l_{stop} is derived as

$$l_{\mathrm{stop}} = \frac{\sqrt{\left(\frac{k_{\mathrm{cog}} l_{\mathrm{rest}}}{m} \right)^2 + \dot{\hat{x}}_{b0}^2 \left(\frac{k_{\mathrm{cog}}}{m} + \frac{g}{z_b} \right)} - \frac{k_{\mathrm{cog}} l_{\mathrm{rest}}}{m}}{\frac{k_{\mathrm{cog}}}{m} + \frac{g}{z_b}}. \tag{31}$$

By setting l_{stop} as (31), the robot can stop just above the supporting point. After the COG of the robot reaches above the supporting point, spring coefficient k_{cog} should be modified to zero. Otherwise, the robot would be pushed back.

The COG of the robot stops with generating arm force when $\hat{E}_f = \hat{E}_{f,\mathrm{equi}}$. In this case, l_{stop} is derived as follows:

$$l_{\mathrm{stop}} = \frac{z_b}{g} \left(\dot{\hat{x}}_{b0} \sqrt{\frac{g}{z_b} - \frac{k_{\mathrm{cog}}}{m}} - \frac{k_{\mathrm{cog}} l_{\mathrm{rest}}}{m} \right). \tag{32}$$

By setting l_{stop} as (32), the COG goes over the supporting point, and then, it stops. The arm keeps on pushing the obstacle after the robot stops.

This strategy of determining the next supporting point is applicable in the case where the robot makes two steps or more during pushing motion.

The walking motion of the robot is always stable on the proposed trajectory since the ZMP of the robot ideally remains to be at the supporting point of the LIPM.

D. Modification of Pushing Force

If k_{cog} is too large, the COG may not go over the supporting point, i.e., the robot will go backward. It is undesirable in many situations. Therefore, in this case, the spring coefficient of the arm should be modified to be smaller.

Applying the following spring coefficient, the robot will stop just above the supporting point:

$$k_{\mathrm{cog}} = m \left(\frac{\dot{x}_c^2}{x_c^2} - \frac{g}{z_b} \right). \tag{33}$$

This spring coefficient is derived by setting $E_f = 0$ in (30). k_{cog} can be calculated when the boundary conditions are given as x_c and $\dot{x}_c$. After the COG of the robot reaches above the supporting point, spring coefficient should be modified to zero. Otherwise, the robot would be pushed back.

In order that the robot stops with generating arm force, k_{cog} should be modified to satisfy $E_f = E_{f,\mathrm{equi}}$. The boundary conditions are given as x_c, x_b, and $\dot{x}_b$. k_{cog} can be calculated as

$$k_{\mathrm{cog}} = \frac{m \left[\frac{2gx_{b0}(x_{b0} - x_c)}{z_b} + \dot{x}_{b0}^2 \left\{ \sqrt{1 + \frac{4gx_c(x_{b0} - x_c)}{z_b \dot{x}_{b0}^2}} - 1 \right\} \right]}{2(x_{b0} - x_c)^2}. \tag{34}$$

In this case, the robot goes over the supporting point, and then, the robot stops in front of the obstacle.

If the obstacle moves, the trajectory of (22) and (23) will be switched to the following trajectory, which is based on constant force f_v. Constant force is exerted in case that the viscous friction between the obstacle and the ground is dominant, i.e.,

$$\bar{x}_b(t) = \left(\bar{x}_{b0} - \frac{f_v}{m\omega^2} \right) \cosh(\omega t) + \frac{\dot{\bar{x}}_{b0}}{\omega} \sinh(\omega t) + \frac{f_v}{m\omega^2} \tag{35}$$

$$\dot{\bar{x}}_b(t) = \left\{ \left(\bar{x}_{b0} - \frac{f_v}{m\omega^2} \right) \sinh(\omega t) + \frac{\dot{\bar{x}}_{b0}}{\omega} \cosh(\omega t) \right\} \omega. \tag{36}$$

$\bar{x}_{b0}$ and $\dot{\bar{x}}_{b0}$ are boundary conditions of $\bar{x}_b(t)$ and $\dot{\bar{x}}_b(t)$ at the moment when the trajectory switches to (35) and (36). Here, "$-$" denotes the coordinate system that is switched after the pushing force becomes constant. With the trajectory of (35) and (36), the stable region of the ZMP has a margin that deals with a quantity of force variation.

V. Simulation

In simulations, each parameter was set as follows: $f_{\max} = 30$ N, $l_r = 0.10$ m, length of stride was 0.1 m, and walking cycle was 1.0 s. An obstacle was assumed as a spring-damper-modeled wall. The trajectory of the swing leg was given by the polynomial that achieved the continuity of acceleration.

Results of the simulations are shown in Figs. 9 and 10. In Fig. 9, the obstacle was set at 0.64 m from the COG of the robot. On the other hand, the obstacle was set at 0.60 m in Fig. 10.

A dash line denotes the moment of contact with the obstacle in each figure. Arm force in Figs. 9(b) and 10(b) was represented only in the left arm. The right arm generated the same amount of force. From Figs. 9(b) and 10(b), pushing motion of spring characteristic was achieved substantially although there is a steady error. The ZMP of the robot is shown in Figs. 9(c) and 10(c). The ZMP existed in the stable region of the plantar

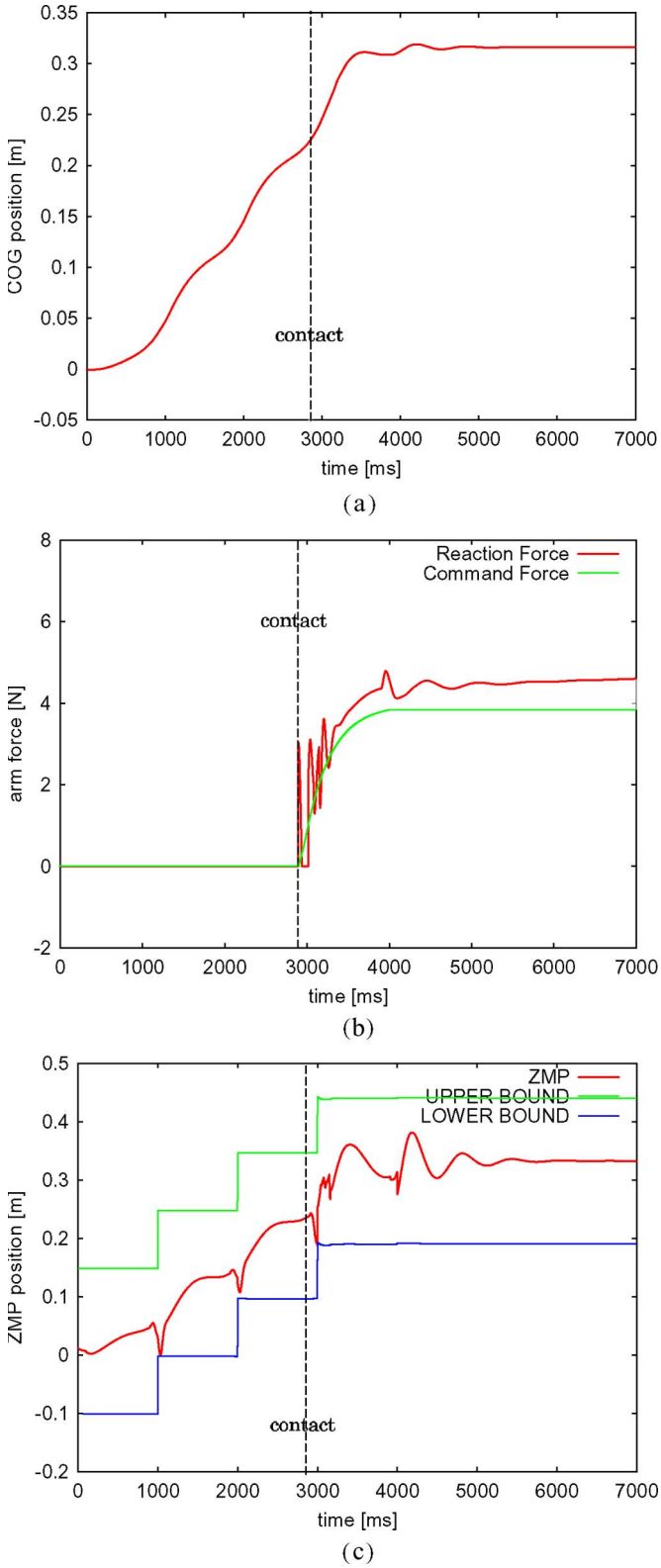

Fig. 9. Simulation results (obstacle was at 0.64 m). (a) COG position in x-axis direction. (b) Arm force. (c) ZMP trajectory.

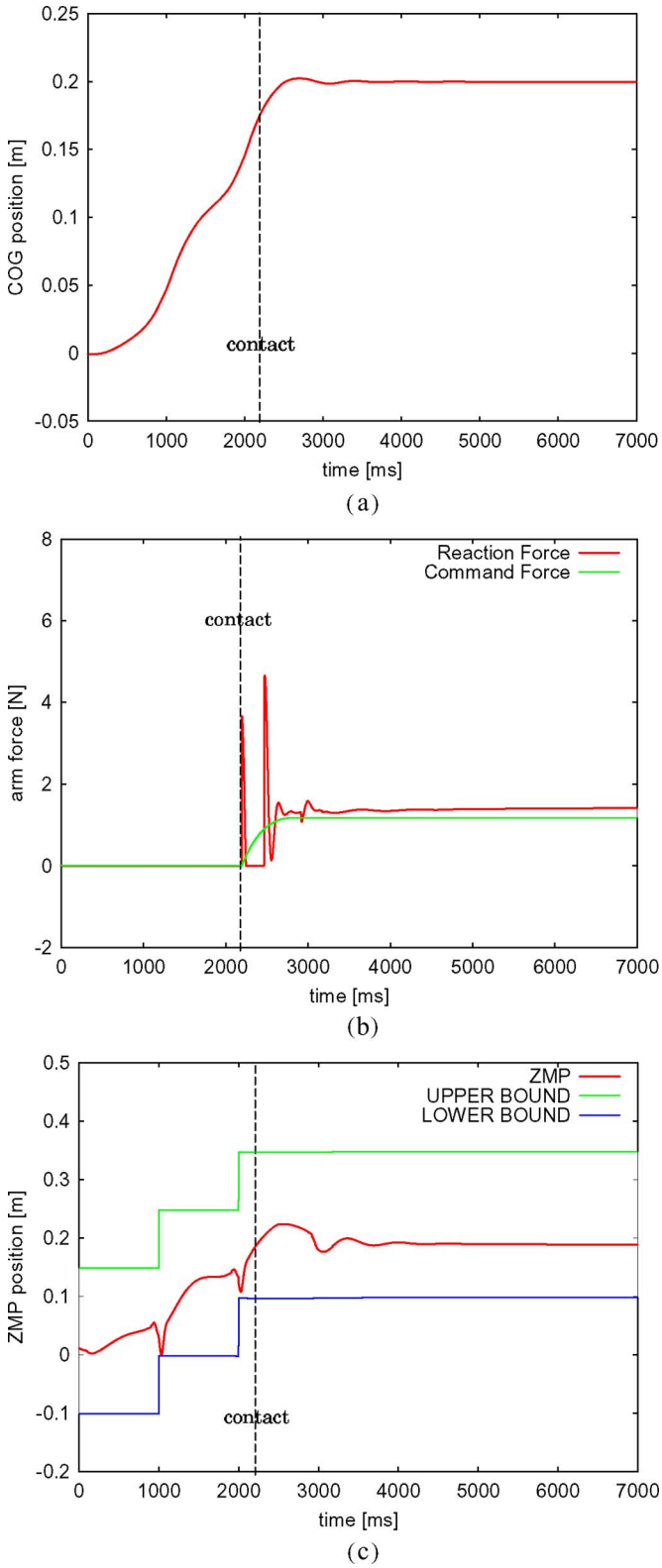

Fig. 10. Simulation results (obstacle was at 0.60 m). (a) COG position in x-axis direction. (b) Arm force. (c) ZMP trajectory.

surface. The fact shows that the robot could remain on walking stably.

As shown in Fig. 9, the robot modified the trajectory smoothly to stop after the robot had contact with the obstacle at around 2.9 s. The length of stride was modified from 0.1 to 0.083 m. The robot could stop around 0.3 m short of the obstacle at 4.1 s. At the moment of the next step after the contact, orbital energy E_f was modified from 0.0064 to 0.0006 $\mathrm{m}^2/\mathrm{s}^2$. The COG of the robot stopped at 0.03 m forward from the supporting point. The robot could remain standing

with constant pushing force of about 4.2 N. Due to contact of the swing leg, the ZMP moved at 4 s.

As shown in Fig. 10, the robot modified the trajectory smoothly to stop after the robot had contact with the obstacle at around 2.2 s. In this simulation, the robot did not make the next step after the contact. The robot could stop around 0.4 m short of the obstacle at 3 s. Orbital energy E_f was modified from 0.0064 to 0.0002 $\mathrm{m}^2/\mathrm{s}^2$ at the moment of contact. The COG of the robot stopped at 0.002 m forward from the supporting point. The robot could remain standing with constant pushing force of about 1.3 N.

From the simulation results, it is verified that the robot can stop short of the obstacle with the proposed method.

VI. Experiment

In the experiment, each parameter was set as follows: $f_{\max} = 15$ N, $l_r = 0.20$ m, length of stride was 0.1 m, and walking cycle was 1.0 s. Compared with simulations, $f_{\max}$ and l_r were set to have a margin of safety. The aluminum board was placed in front of the robot as an obstacle.

The results of the experiment are shown in Fig. 11. The robot started to walk at 2 s. The robot had contact with the obstacle at around 3.6 s. Then, the robot switched to the proposed trajectory. The length of stride was modified into 0.077 m. The robot could stop around 0.1 m short of the obstacle at 4.8 s. Orbital energy E_f was modified from 0.0064 to 0.0015 $\mathrm{m}^2/\mathrm{s}^2$, and k_{cog} was set to be equal to 102 N/m at the moment of contact.

As shown in Fig. 11(a), the robot modified the trajectory smoothly to stop. External force was estimated by the reaction force observer [17]. From Fig. 11(b), pushing motion of spring characteristic was achieved substantially although there was an offset on estimated force (about -2 N). The robot could remain standing with constant pushing force of about 7 N. The pushing force decreased once at 4.0 s. We consider its reason as follows: The robot had contact with the obstacle at 3.6 s, and then, the aluminum board was bent mechanically. Therefore, the arm force was decreased at around 4.0 s. The ZMP of the robot is shown in Fig. 11(c). The ZMP existed in the stable region of the plantar surface.

From the experimental results, it is verified that the robot can stop short of the obstacle with the proposed method.

VII. Conclusion

This paper has described the pushing motion of the humanoid robot. The robot utilizes the arms to generate the desired walking motion. We extended orbital energy for pushing motion. Extended orbital energy detects whether the robot can stop or not. Appropriate landing points can be determined from the orbital energy.

The proposed method is given as follows: At first, the robot contacts the obstacle with compliance, then increases the arm force. The robot can stop short of the obstacle if the obstacle is unmovable like a wall, then the robot avoids collision with the obstacle. With the proposed method, the robot utilized arm force to stop or to keep on walking with compliance to the obstacle without losing walking stability. If the obstacle is movable like a door, the robot pushes it and can continue walking.

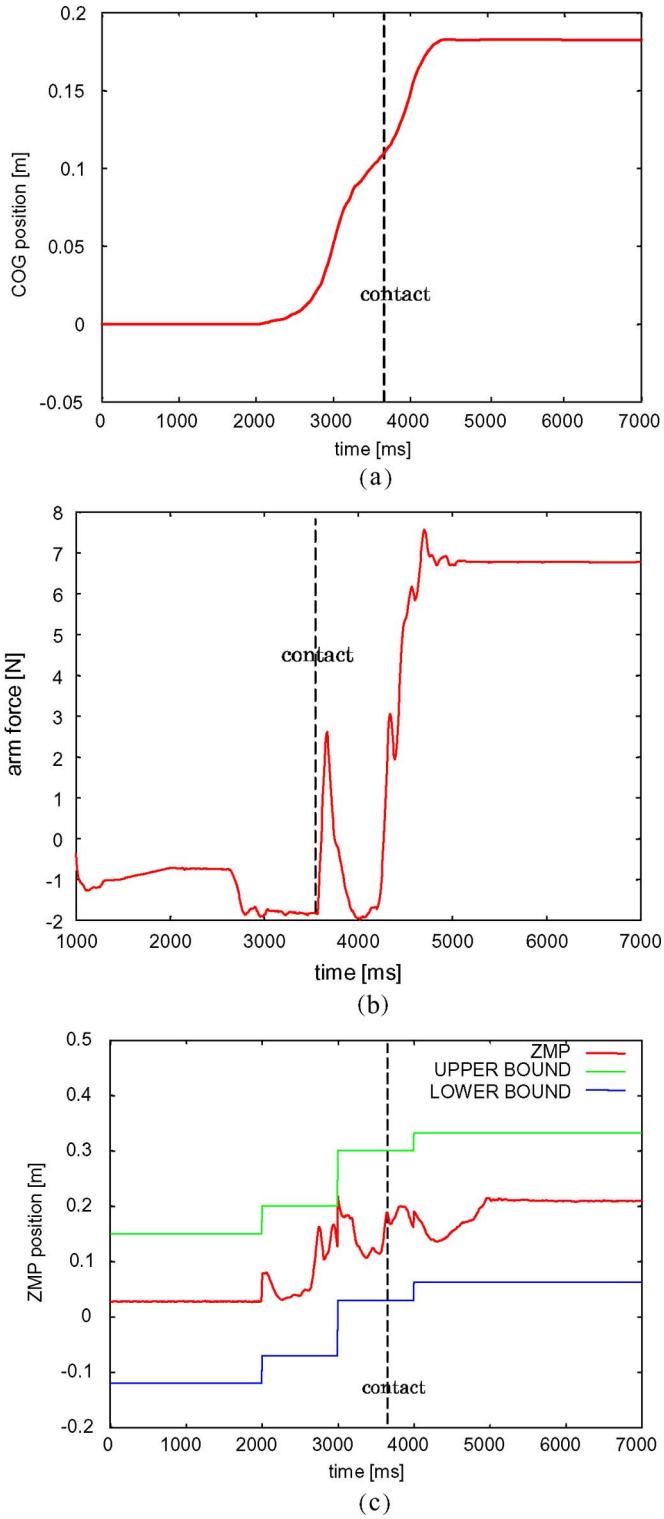

Fig. 11. Experimental results. (a) COG position in x-axis direction. (b) Arm force. (c) ZMP trajectory.

In this paper, the upper body and the lower body are considered as a whole system to achieve the desired motion. We also expect that humanoid robots will do a lot of work as a unified system.

REFERENCES

[1] K. Löffler, M. Gienger, F. Pfeiffer, and H. Ulbrich, "Sensors and control concept of a biped robot," *IEEE Trans. Ind. Electron.*, vol. 51, no. 5, pp. 972–980, Oct. 2004.

[2] K. C. Tan, Y. J. Chen, K. K. Tan, and T. H. Lee, "Task-oriented developmental learning for humanoid robots," *IEEE Trans. Ind. Electron.*, vol. 52, no. 3, pp. 906–914, Jun. 2005.

[3] S. Kajita, T. Nagasaki, K. Kaneko, K. Yokoi, and K. Tanie, "A hop towards running humanoid biped," in *Proc. IEEE ICRA*, 2004, vol. 1, pp. 629–635.

[4] T. Nagasaki, S. Kajita, K. Kaneko, K. Yokoi, and K. Tanie, "A running experiment of humanoid biped," in *Proc. IEEE/RSJ Int. Conf. IROS*, 2004, vol. 1, pp. 136–141.

[5] S. Kajita, T. Nagasaki, K. Yokoi, K. Kaneko, and K. Tanie, "Running pattern generation for a humanoid robot," in *Proc. IEEE ICRA*, 2002, vol. 3, pp. 2755–2761.

[6] F. Pfeiffer, K. Löffler, and M. Gienge, "The concept of jogging JOHNNIE," in *Proc. IEEE ICRA*, 2002, vol. 3, pp. 3129–3135.

[7] K. Harada, S. Kajita, F. Kanehiro, K. Fujiwara, K. Kaneko, K. Yokoi, and H. Hirukawa, "Real-time planning of humanoid robot's gait for force controlled manipulation," in *Proc. IEEE ICRA*, 2004, vol. 1, pp. 616–622.

[8] K. Harada, S. Kajita, K. Kaneko, and H. Hirukawa, "Pushing manipulation by humanoid considering two kinds of ZMPs," in *Proc. IEEE ICRA*, 2003, vol. 2, pp. 1627–1632.

[9] K. Harada, S. Kajita, K. Kaneko, and H. Hirukawa, "ZMP analysis for arm/leg coordination," in *Proc. IEEE/RSJ Int. Conf. IROS*, 2003, vol. 1, pp. 75–81.

[10] Y. Hwang, A. Konno, and M. Uchiyama, "Whole body cooperative tasks and static stability evaluations for a humanoid robot," in *Proc. IEEE/RSJ Int. Conf. IROS*, 2003, vol. 2, pp. 1901–1906.

[11] H. Yoshida, K. Inoue, T. Arai, and Y. Mae, "Mobile manipulation of humanoid robots—Analysis of manipulability and stability in mobile manipulation," in *Proc. IEEE/RSJ Int. Conf. IROS*, 2000, vol. 3, pp. 1924–1929.

[12] H. Yoshida, K. Inoue, T. Arai, and Y. Mae, "Mobile manipulation of humanoid robots—Method of adjusting leg motion for improvement of arm's manipulability," in *Proc. IEEE/RSJ Int. Conf. IROS*, 2001, vol. 1, pp. 266–271.

[13] K. Terada, Y. Ohmura, and Y. Kuniyoshi, "Analysis and control of whole body dynamic humanoid motion—Towards experimental on a roll-and-rise motion," in *Proc. IEEE/RSJ Int. Conf. IROS*, 2003, vol. 2, pp. 1382–1387.

[14] T. Yamamoto and Y. Kuniyoshi, "Stability and controllability in a rising motion: A global dynamics approach," in *Proc. IEEE/RSJ Int. Conf. IROS*, 2002, vol. 3, pp. 2467–2472.

[15] S. Kajita, T. Yamamura, and A. Kobayashi, "Dynamic walking control of a biped robot along a potential energy conserving orbit," *IEEE Trans. Robot. Autom.*, vol. 8, no. 4, pp. 431–438, Aug. 1992.

[16] M. Morisawa, Y. Fujimoto, T. Murakami, and K. Ohnishi, "A walking pattern generation for biped robot with parallel mechanism by considering contact force," in *Proc. IEEE IECON*, 2001, vol. 3, pp. 2184–2189.

[17] T. Murakami, F. Yu, and K. Ohnishi, "Torque sensorless control in multidegree-of-freedom manipulator," *IEEE Trans. Ind. Electron.*, vol. 40, no. 2, pp. 259–265, Apr. 1993.

Eijiro Ohashi received the B.E. and M.E. degrees in system design engineering from Keio University, Yokohama, Japan, in 2003 and 2005, respectively.

He is currently a Researcher with Canon Inc., Tokyo, Japan. His research interests include robotics and motion control.

Takahiro Aiko received the B.E. and M.E. degrees in system design engineering from Keio University, Yokohama, Japan, in 2003 and 2005, respectively.

He is currently a Researcher in the Plant Control Department, East Japan Works, JFE Steel Corporation, Kawasaki, Japan. His research interests include motion control of biped robots.

Toshiaki Tsuji (S'05) received the B.E. degree in system design engineering and the M.E. degree in integrated design engineering from Keio University, Yokohama, Japan, in 2001 and 2003, respectively. He is currently working toward the Ph.D. degree at the same university.

His research interests include robotics, motion control, decentralized control, and haptics.

Hiroaki Nishi (M'02) received the B.E., M.E., and Ph.D. degrees in electrical engineering from Keio University, Yokohama, Japan, in 1994, 1996, and 1999, respectively.

He was a Researcher in the Central Research Laboratory, Network Platform Research Department, Hitachi Ltd., Tokyo, Japan, in 2002. He is currently a Lecturer in the Department of System Design Engineering, Faculty of Science and Technology, Keio University. His research interests include networks for high-performance computing, robotics, and haptics.

Kouhei Ohnishi (S'78–M'80–SM'00–F'01) received the B.E., M.E., and Ph.D. degrees in electrical engineering from the University of Tokyo, Tokyo, Japan, in 1975, 1977, and 1980, respectively.

Since 1980, he has been with the Department of System Design Engineering, Faculty of Science and Technology, Keio University, Yokohama, Japan. His research interests include robotics, motion control, and haptics.

Dr. Ohnishi was the recipient of the Best Paper Award at IECON'85, IECON'92, and IECON'93.